

## Numerical Simulation of Impulsive Water Waves Generated by Subaerial and Submerged Landslides Incidents in Dam Reservoirs

Vafa Khoolosi <sup>a\*</sup>, Sedat Kabdaşlı <sup>b</sup>

<sup>a</sup> PhD student, Department of Civil Engineering, Istanbul Technical University, Istanbul, Turkey.

<sup>b</sup> Prof. of Department of Civil Engineering, Istanbul Technical University, Ayazağa Campus, Istanbul, Turkey.

Received 16 September 2016; Accepted 24 October 2016

### Abstract

The water wave generation by a freely falling rigid body is examined in this paper. Landslides on the margins of dam reservoirs may generate large waves that can produce flooding over the banks or overtopping the dam crest. In the present investigation, landslide generated waves are studied using a numerical model based on Navier-Stokes equations. Impulse wave amplitude, period, energy is studied in this work. The effects of bed slope angle on energy conversion from slide into wave are also investigated, and the numerical model we used in this study is the full three dimensional commercial code Flow-3D. Results of the Navier-Stokes model show that waves generated are highly dependent upon the details of slide mechanism and kinematics. Numerical solutions for the velocity fields, pressure distributions, and turbulence intensities in the vicinity of the falling rigid body are also presented. Results show that the general pattern of wave in all cases is the same but the amplitude and period are different. Data analysis shows that the maximum wave crest amplitude in subaerial induced waves is strongly affected by bed slope angle, landslide impact velocity, thickness, kinematics and deformation and by landslide shape.

*Keywords:* Impulsive Water Waves; Subaerial; Submerge; landslide; Dam Reservoir.

### 1. Introduction

Empirical studies of water waves generated by underwater landslides have been conducted by Wiegel [1], Iwasaki [2], Heinrich [3], and Watts [4]. All these studies considered the motion of solid blocks or boundaries. Iwasaki conducted a wide variety of numerical studies for water waves generated by solid underwater landslides of various geometries, using the linear shallow water wave equations. Heinrich performed similar studies using a finite volume discretization of the Navier–Stokes equations; these computations agreed remarkably well with experimental results. Jiang and Leblond [5, 36] developed a model of deformable underwater landslides, generating waves governed by the nonlinear shallow water wave equations. Verriere and Lenoir [6] solved a linearized velocity potential problem to describe water waves generated by perturbations around a circular island. Harbitz [7] used the linear shallow water wave equations to model the Storegga landslide as a sliding solid block generating waves [14, 35].

Dams are usually built in valleys where active erosion is present, and some are in active earthquake areas. Therefore, reservoirs can be vulnerable to landslides activated by earthquakes or by heavy rains and they could generate large waves that can produce flooding over the banks or overtopping the dam crest [8]. Water waves generated by the sliding movement of land volumes (landslides or slumps) into nearby water bodies are of great interest to coastal and ocean engineering. Landslides are natural phenomena that occur under certain conditions such as earthquakes, underwater mass movement, heavy rainfalls and storms, erosion and water fluctuations [10]. In such events, landslides are capable of generating several types of long waves, such as tsunamis, due to energy transfer to the

\* Corresponding author: [vafa1881@yahoo.com](mailto:vafa1881@yahoo.com)

water. In the present study we are mainly concerned for long waves generated with the impact of submarine and subaerial slides into water volumes which are assumed initially at rest [15, 33].

The surface waves generated by underwater landslides are governed by many parameters describing the landslide geometry and kinematics. Most coastal landslides can essentially be idealized as underwater bodies sliding along a sloping bottom [10, 34]. In such cases, and particularly for small initial submergence of the landslide, the earlier studies showed that complex nonlinear interactions may occur between surface waves and the underwater body. One important characteristic of underwater landslides is the water run-up/run-down motion induced at the shoreline [8, 37]. Predicting this run-up is of prime importance for assessing risks and magnitude of flooding in coastal areas subjected to underwater landslides. Earlier studies considered idealized cases and/or neglected important effects for the early stages of underwater landslides, such as the strong free surface nonlinearity. Some more realistic studies were based on only one simulation which precludes the many sensitivity analyses required for a comprehensive and reliable run-up prediction [15, 32].

Previous studies on submarine and subaerial landslides (see Figure 1. for the classification) tried to understand the influence of the landslide parameters on the generated waves. Murty [9] analytically calculated the wave height generated by a submarine landslide, assuming that the potential energy of the slide was transferred in a solitary wave. Pelinovsky & Poplavsky [9] and Watts [4] calculated analytically the final velocity of a submerged solid sliding down a slope. Experimental investigations were carried out using solid bodies: Law & Brebner [9] used a solid box to generate subaerial landslides; they concluded that the leading wave is always the most significant. Kamphuis & Bowering [9] used a tray rolling down a roller ramp. They observed that the main parameters to evaluate the wave height were the Froude number for the impact velocity and the slide volume. Based on their experiments using solid bodies, Walder et al. [12] demonstrated that the shape and the height of the generated wave in near field depend on the water depth, the volume of the slide and the duration of the submerged landslide motion. Enet et al. [12] performed experiments dealing with 3-D rigid underwater landslides. Experiments with granular materials were conducted to study the influence of the slide rigidity. Fritz [12] used a pneumatic landslide generator to study subaerial landslide impacts with Froude number  $Fr > 1$ . A particle image velocimetry (PIV) method were used to analyses the interactions between the slide and water. From all these experiments, predictive equations on wave amplitude, wave period, and wavelength and propagation velocity were provided using multiple regressions with very good correlation coefficients. An extension to 3-D cases was performed by Mohammed & Fritz [12]. Ataie-Ashtiani & Nik-Khah [13] performed laboratory experiments on impulse waves generated by rigid and deformable slide masses. They showed that the maximum wave crest amplitude is strongly affected by the landslide impact velocity, thickness, deformation and weakly affected by the shape. Several numerical methods were used to understand and analyses these observations. Heinrich et al. [11, 28] used non-linear shallow water equations to model fluid and slide motions. Monaghan & Kos [9] used the smoothed particle hydrodynamics (SPH) to simulate the interactions between sliding masses and water for subaerial cases. These single-phase flow simulations reproduce successfully some challenging features, like the reverse plunging breaking and a dimensional analysis were performed on the amplitude of the wave assuming like Murty [9] that the potential energy of the weighted box is transferred in the generated solitary wave [14, 27].

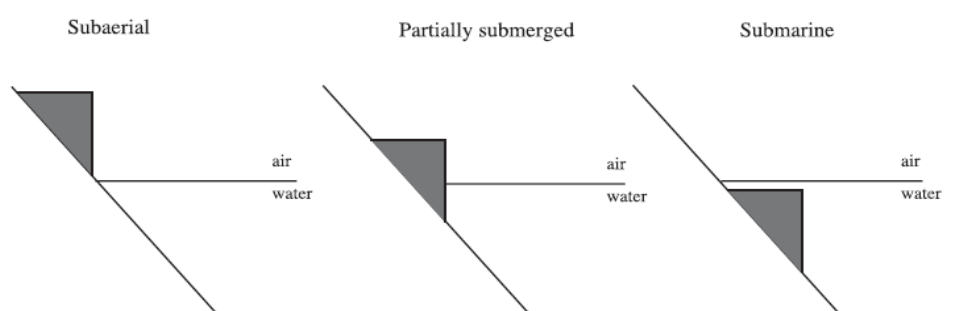


**Figure 1. Landslide generated tsunami wave's classification. This classification is based on the initial position of the landslide: subaerial, partially submerged or submarine**

Heinrich [2, 26] used a finite difference technique to solve incompressible Navier–Stokes equations for the simulation of submarine and subaerial landslides. More recently, Fernandez-Nieto et al. [2, 25] used a Savage–Hutter type model to describe both deformed landslide and associated waves. Abadie et al. [11, 24] considered a multiple-fluid Navier-Stokes model using a finite volume discretization and a VOF (volume of fluid) method to track the interface and describe the interactions between slide/air/water.

Last study presents the experimental results of impulsive waves caused by subaerial landslides that we use in this thesis. A wide range of effective parameters are considered and studied by performing 120 laboratory tests. Considered slide masses are both rigid and deformable. The effects of bed slope angle, water depth, slide impact velocity,

geometry, shape and deformation on impulse wave characteristics have been inspected. The impulse wave features such as amplitude, period and also energy conversion are studied. Experiments were set-up in a 2.5 m wide, 1.8 m deep and 25 m long wave tank at Sharif University of Technology by B. Ataie-Ashtiani (2015) and A. Nik-Khah (2013). Recorded data at near field and far field shows general pattern of generated subaerial impulse wave consists of a wave train with positive leading wave amplitude. Second wave crest of this train has the maximum amplitude that followed by smaller oscillatory waves. Results of experiments show that the general pattern of wave in all cases is the same but the amplitude and period are different [39]. The main objective of this work is to study the characteristics of impulsive waves generated by subaerial landslides in a range of parameters that covers some of the limitations in previous works.

## 2. Numerical Model

### 2.1. Governing Equations

Surface wave generation by a moving slide is affected by the water depth, gravity, and fundamental characteristics of the slide [17, 29]. The principal mechanism for energy transfer from the slide motion to the surface waves, water displacement, is readily incorporated using the long-wave (shallow-water) approximation [38]. The main assumptions for the present models (viscous and rigid-body) are the following:

- (1) The surface waves and slides satisfy the long-wave (hydrostatic) approximation, implying that the wavelength of the water waves is much greater than the water depth, and that the width and length of the viscous slide is much greater than the slide thickness.
- (2) The viscous slide is an incompressible, isotropic, laminar, quasi-steady viscous fluid; the viscous regime is rapidly reached in any failure and in the steady-state regime, the horizontal velocities have a parabolic vertical profile.
- (3) The rigid-body slide moves as a non-deformable body with given friction.
- (4) The seawater is an incompressible in viscous fluid.

We use standard Cartesian coordinates  $x, y, z$  with  $z$  measured vertically upward. For time  $t$ , the upper (water) layer consists of seawater with density  $\rho_1$ , surface elevation  $\eta(x, y; t)$ , and horizontal velocity  $u$  with components  $u$  and  $v$  (Figure 2a). The lower layer consists of viscous sediments (or rigid body) having density  $\rho_2$ , dynamic viscosity  $\mu$  (or friction coefficient  $k$  in case of a rigid body), and horizontal velocity  $U$  with components  $U$  and  $V$ . Both the slope and the slide have small angles, so the motion is essentially horizontal. The slide is bounded by an upper surface  $z = -h(x, y; t)$  and the seabed surface  $z = -h_b(x, y)$ , giving the slide thickness as  $D(x, y; t) = h_b(x, y) - h(x, y; t)$ .

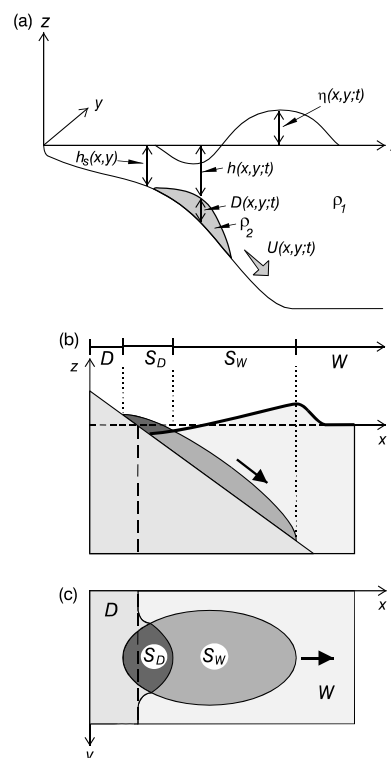


**Figure 2.** (a) Sketch of a submarine landslide with density  $\rho_2$ , thickness  $D$ , and water depth  $h$ , and associated surface waves of height  $\eta$ . (b) Side view and (c) plan view of a combined subaerial and submarine slide (see the text for description of the letters)

A schematic of the computational domain for a landslide with a subaerial component is presented in Figure 2. The domain consists of four zones: (1) The *dry* coastal area,  $D$ ; (2) the *dry* portion of the slide,  $S_D$ , corresponding to the subaerial part of the slide; (3) the *wet* portion of the slide,  $S_w$ , corresponding to the submarine part of the slide; and (4) the *water*,  $W$ . The numerical model must account for the time-varying changes in the areas and locations of these zones [21, 22].

## 2.2. Viscous Slide

Our purpose is to construct the non-linear, vertically integrated Navier-Stokes equations for the landslide. We assume that the landslide occupies a domain from  $z=0$  to  $z=D$ . Following JLB94, we assume that the landslide rapidly reaches a steady shape so that we can use a locally parabolic approximation in the vertical to describe the horizontal velocities, and; specifically,

$$U_m(x, y, z; t) = U(x, y; t)(2\xi - \xi^2) \quad (1a)$$

$$V_m(x, y, z; t) = V(x, y; t)(2\xi - \xi^2) \quad (1b)$$

Where  $\xi = (z + h_s)/D$ . The equations for conservation of mass and momentum for a viscous submarine slide have the form [30, 20]:

$$\frac{\partial D}{\partial t} + \frac{2}{3} \left[ \frac{\partial(DU)}{\partial x} + \frac{\partial(DV)}{\partial y} \right] = 0 \quad (2)$$

$$\rho_2 \frac{2}{3} \left[ \frac{\partial U}{\partial t} - \frac{1}{5} \frac{U}{D} \frac{\partial D}{\partial t} + \frac{4}{5} \left( U \frac{\partial U}{\partial x} + V \frac{\partial U}{\partial y} \right) \right] = -g \left[ (\rho_2 - \rho_1) \left( \frac{\partial D}{\partial x} - \frac{\partial h_s}{\partial x} \right) + \rho_1 \frac{\partial \eta}{\partial x} \right] - \frac{2\mu U}{D^2} \quad (3a)$$

$$\rho_2 \frac{2}{3} \left[ \frac{\partial V}{\partial t} - \frac{1}{5} \frac{V}{D} \frac{\partial D}{\partial t} + \frac{4}{5} \left( U \frac{\partial V}{\partial x} + V \frac{\partial V}{\partial y} \right) \right] = -g \left[ (\rho_2 - \rho_1) \left( \frac{\partial D}{\partial y} - \frac{\partial h_s}{\partial y} \right) + \rho_1 \frac{\partial \eta}{\partial y} \right] - \frac{2\mu V}{D^2}. \quad (3b)$$

The continuum Equation 2. is the same as in the JLB94 model. However, the momentum Equations 3a. and 3b. are slightly different from those presented by Jiang and LeBlond [17, 19] as a result of corrections we have made to several of the constant coefficients in the terms in the square brackets on the left-hand sides of these equations. Numerical experiments we have conducted show that the small errors in these advective terms in the JLB94 model may cause 20-25% errors in computed tsunami heights.

For a subaerial slide, it is useful to introduce a new variable  $h_w$ , the full water thickness ( $h_w = \eta + h = \eta - D + h_s$ ), and to present Equations 3a. and 3b. in the form:

$$\rho_2 \frac{2}{3} \left[ \frac{\partial U}{\partial t} - \frac{1}{5} \frac{U}{D} \frac{\partial D}{\partial t} + \frac{4}{5} \left( U \frac{\partial U}{\partial x} + V \frac{\partial U}{\partial y} \right) \right] = -g \left[ \rho_2 \left( \frac{\partial D}{\partial x} - \frac{\partial h_s}{\partial x} \right) + \rho_1 \frac{\partial h_w}{\partial x} \right] - \frac{2\mu U}{D^2}; \quad (4a)$$

$$\rho_2 \frac{2}{3} \left[ \frac{\partial V}{\partial t} - \frac{1}{5} \frac{V}{D} \frac{\partial D}{\partial t} + \frac{4}{5} \left( U \frac{\partial V}{\partial x} + V \frac{\partial V}{\partial y} \right) \right] = -g \left[ \rho_2 \left( \frac{\partial D}{\partial y} - \frac{\partial h_s}{\partial y} \right) + \rho_1 \frac{\partial h_w}{\partial y} \right] - \frac{2\mu V}{D^2}. \quad (4b)$$

For the subaerial zone,  $S_D$ , we have the particular case of zero water thickness,  $h_w = 0$  for which Equations 4a. and 4b. describe slide motion on a dry coast.

The above equations are solved subject to the condition of zero transport through the coastal boundary ( $G$ ) and require that the slide does not cross the outer (open) boundary ( $\Gamma$ ). The condition of no volume transport through the coast gives

$$U_n = 0 \text{ on } G \quad (5)$$

Where  $U_n$  is the normal slide velocity [20, 30].

## 2.3. Rigid-Body Slide

The rigid-body model assumes that the shape and dimensions of the initial slide remain invariant during the slide motion. All points of the rigid body move with the same velocity  $U=U(t)$  and the position of the slide changes with time through the relation:

$$D(x, y; t) = D_0(x - X(t), y - Y(t)), \quad (6)$$

Where  $D_0$  is the initial slide distribution, and  $X = \int_0^t U dt$ ,  $Y = \int_0^t V dt$ . In solving the equations of motion, we further assume that: (1) Bottom friction on the slide is proportional to the normal pressure,  $P$ ; (2) there are no hydraulic forces (form drag) on the slide; and (3) the bottom slope is small,  $|\nabla h| \ll 1$ . Under these assumptions, the momentum

equation of the slide becomes;

$$\rho_2 \frac{dU}{dt} \iint_S D ds = \tilde{N} h \times P - k \frac{U}{|U|} P \quad (7)$$

Where  $k$  is the nondimensional coefficient of kinetic friction (the Coulomb friction coefficient),  $S$  is the surface area of the slide,

$$P = g \iint_S (\rho_1 \eta + \Delta \rho D) ds \quad (8)$$

And  $\Delta \rho = \rho_2 - \rho_1$  is the density difference between the slide and seawater. The boundary conditions for the rigid slide are the same as for the viscous slide [20, 30].

## 2.4. Surface Wave

For surface waves generated by a submarine slide, the water motions are nearly horizontal and the pressure is hydrostatic (long-wave approximation). The nonlinear shallow-water equations then have the form [17, 31]:

$$\frac{\partial h_w}{\partial t} + \frac{\partial(h_w u)}{\partial x} + \frac{\partial(h_w v)}{\partial y} = 0; \quad (9)$$

$$\frac{\partial u}{\partial t} + u \frac{\partial u}{\partial x} + v \frac{\partial v}{\partial y} = -g \frac{\partial \eta}{\partial x}; \quad (10a)$$

$$\frac{\partial v}{\partial t} + u \frac{\partial v}{\partial x} + v \frac{\partial v}{\partial y} = -g \frac{\partial \eta}{\partial y}, \quad (10b)$$

Which are applicable to wet zones,  $S_w$  and  $W$  (see Figure 2c). At the shore (boundary  $G$ ), we assume a vertical wall with zero normal velocity:

$$u_n = 0 \quad \text{on } G. \quad (11)$$

At the open boundary ( $\Gamma$ ), the one-dimensional radiation condition for outgoing waves is:

$$\frac{\partial \eta}{\partial t} = \text{sgn} \left( \frac{\partial \eta}{\partial t} \right) \sqrt{gh - \left[ \left( \frac{\partial \eta}{\partial x} \right)^2 + \left( \frac{\partial \eta}{\partial y} \right)^2 \right]} \quad (12)$$

At the initial time  $t = 0$ , both the slide and the sea surface are at rest.

## 3. Modeling of Surface Water Waves

### 3.1. Introduction

Flow-3D software package is used to examine the hydraulic performance of the system. The fundamental laws of mass, momentum and energy conservation were adopted in which the finite difference method was applied to solve these equations. The numerical model we will use in this study is the full three dimensional commercial code Flow-3D. The model has already been successfully used to study the interaction of waves and structures. Flow-3D, developed by Flow Sciences, is a general purpose computational fluid dynamics simulation software package developed at Los Alamos National Laboratory in the 1960s and 1970s. The basis of the solver is a finite volume or finite difference formulation, in an Eulerian framework, of the equations describing the conservation of mass, momentum, and energy in a fluid. The physical scale model of this study has been carried out to provide a data set to verify the three-dimensional numerical model. In order to make a good comparison possible, the numerical model should use the similar model parameters as have been used in the physical scale model. So, we now simulate the generation of waves by a subaerial landslide, with Flow-3D software. The obtained results by the numerical method include the amounts of wave height, time history of free surface fluctuations in different locations, and wave propagation for different landslide geometries [16, 38]. In Flow-3D, there are five turbulence models available: the Prandtl mixing length model, the one-equation, the two-equation  $k-\varepsilon$  and RNG models, and a large eddy simulation, LES, model. I used turbulence model based on Renormalization-Group (RNG) methods. This approach applies statistical methods to the derivation of the averaged equations for turbulence quantities, such as turbulent kinetic energy and its dissipation rate.

### 3.2. Numerical Models

Numerical models were set-up in a 2.5 m wide, 1.8 m deep and 25 m long wave tank with Flow-3D software. Bed slope angle is 45 degrees. All of the simulations in this study are performed in three rigid blocks, the shapes of rigid slides have been set up with triangular section, rectangular section and circular section and the shape of granular slide

has been set up with circular section. The volume of rectangular section is  $3900 \text{ cm}^3$ , triangular section is  $3900 \text{ cm}^3$  and circular section is  $3900 \text{ cm}^3$ . Mass density of all sections defined  $1.9 \text{ kg/m}^3$  (Figure 3.a). Figure 3.b shows the geometry details of three rigid blocks.

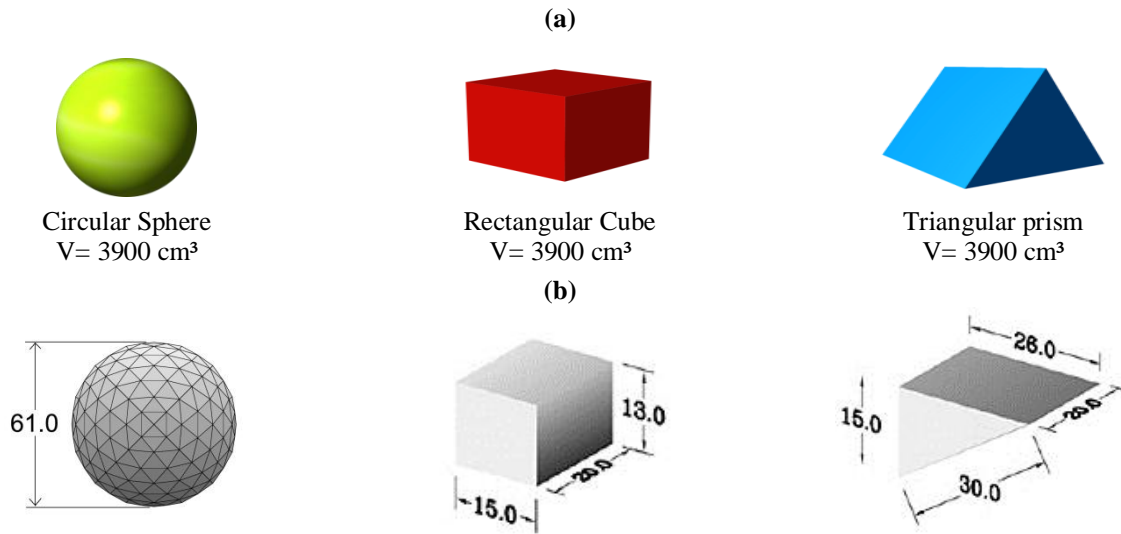


Figure 3. (a) Schematic of three rigid blocks, (b) geometry details of three rigid blocks

Table 1. shows some information about the total mesh size and the typical sizes of the grid elements. Also total number of real cell is 170000. The CPU time used in each simulation is 40 min. In this study we used viscous flow and laminar model for simulations (Figure 4).

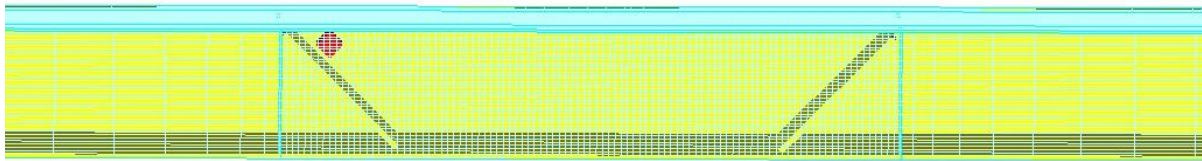


Figure 4. View of grid and mesh blocks

Table 1. Grid information for mesh blocks

Mesh information	X direction	Y direction	Z direction
Number of real cells	28	160	38
Minimum cell size (cm)	8	6	5
Maximum cell size (cm)	11	50	5

Figure 5. shows the top view of numerical models of Flow-3D software. This Figure shows Subaerial slide by red color and two cross section of A-A and B-B.

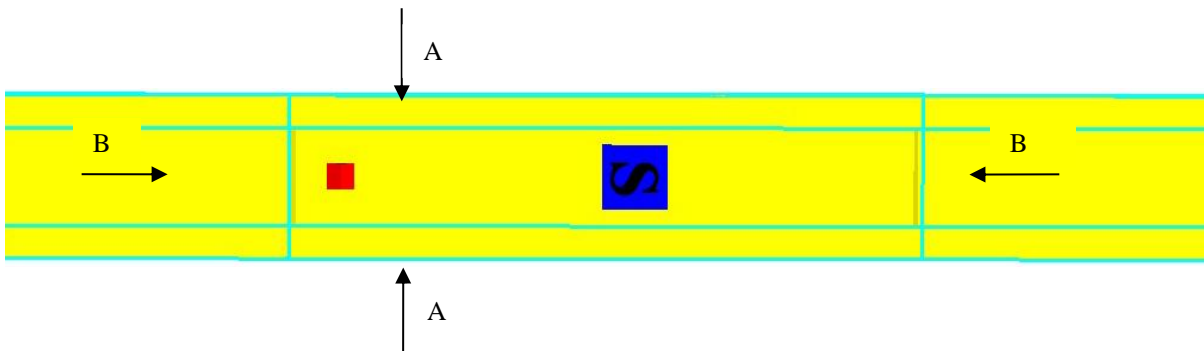


Figure 5. Top view of numerical models

Figure 6. shows the Front view of numerical models of Flow-3D software.

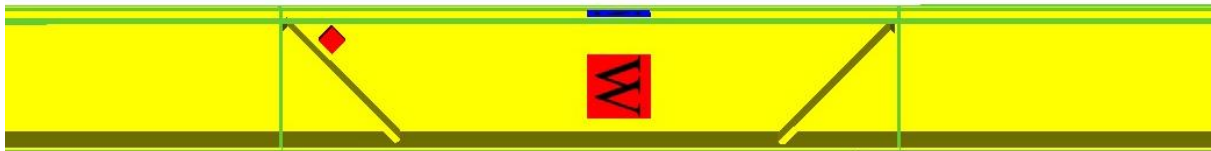


Figure 6. Front view of numerical models

Figure 7. shows the 3D view of numerical model of Flow-3D software.

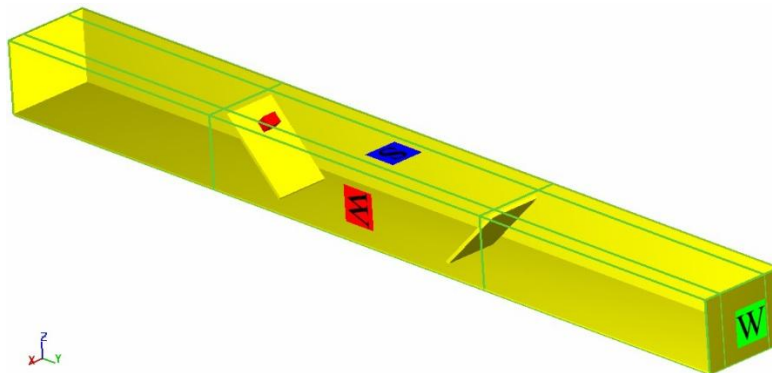


Figure 7. 3D view of numerical models

Figure 8. shows the Top, Front view of numerical model of Flow-3D software.

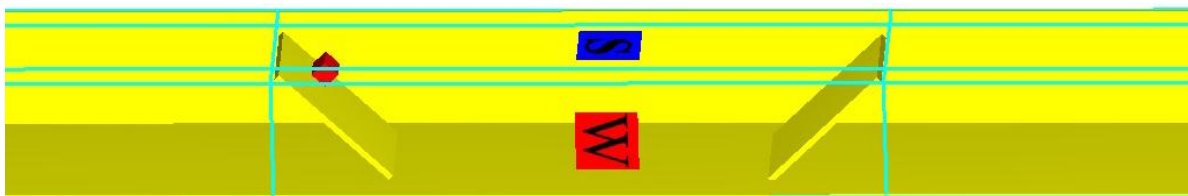


Figure 8. Top and Front view of numerical models

Figure 9. shows 3D top view of numerical models full of water.

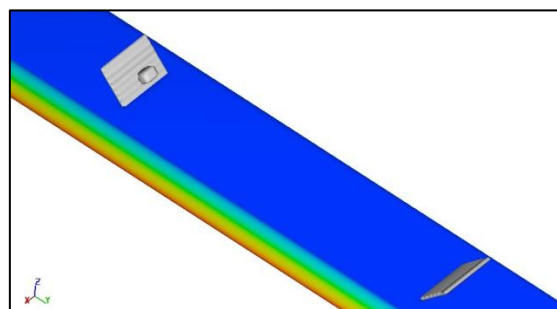
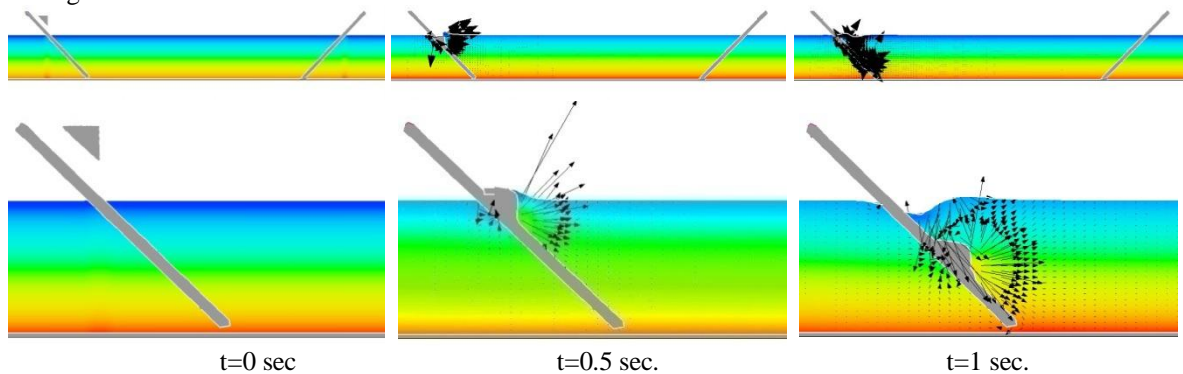


Figure 9. 3D top view of numerical models full of water

Velocity vectors at  $t=0$ ,  $t=0.5$  and  $t=1$  sec. for subaerial different landslide geometries (cross section B-B) are shown in Figure 10.

Triangular:



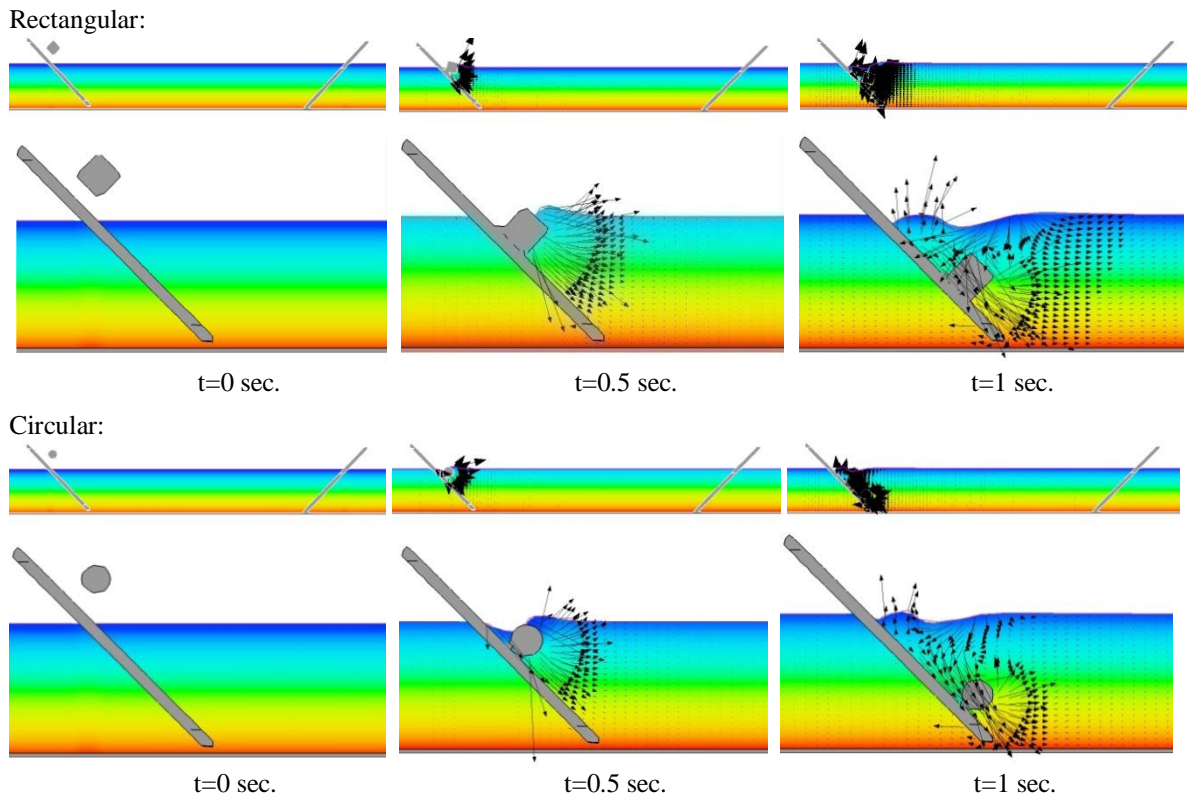


Figure 10. Velocity vectors for subaerial different landslide geometries

Numerical results of wave amplitudes over time in locations of  $y=7m$  (cross section A-A) for different types of landslide geometries are presented in Figure 11. It is shown that the wave's amplitude has the highest and lowest values in triangular, rectangular and circular shapes, respectively. This analysis shows that the water level has changed lowest in circular sphere, and this indicates that the circular shape less effective compared with other forms to create the water waves.

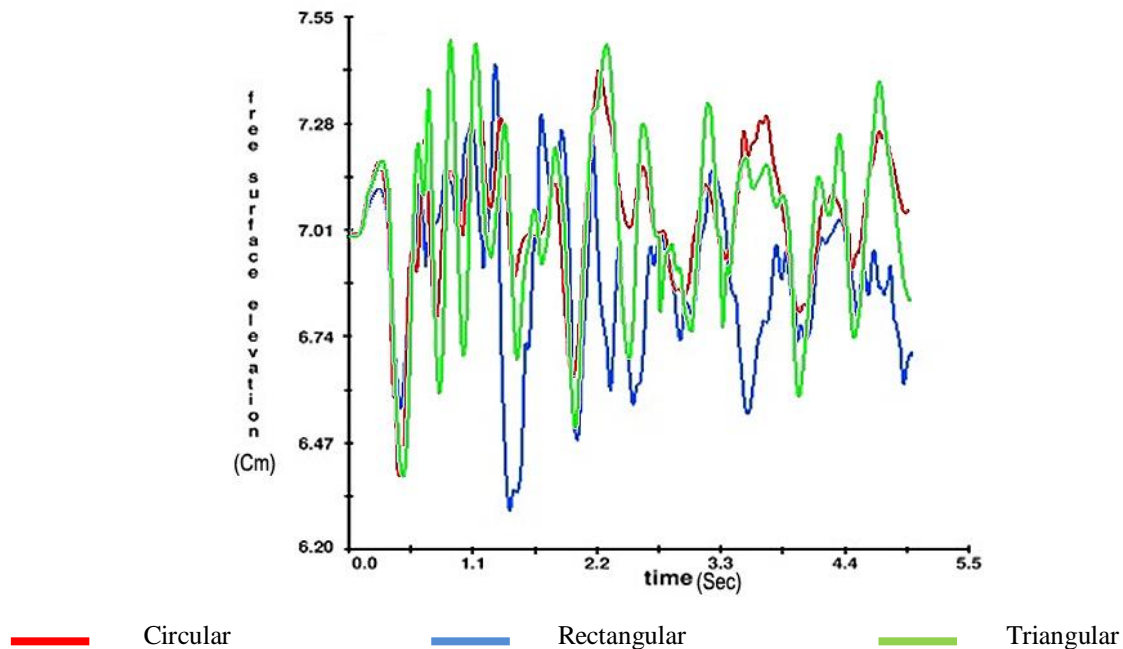
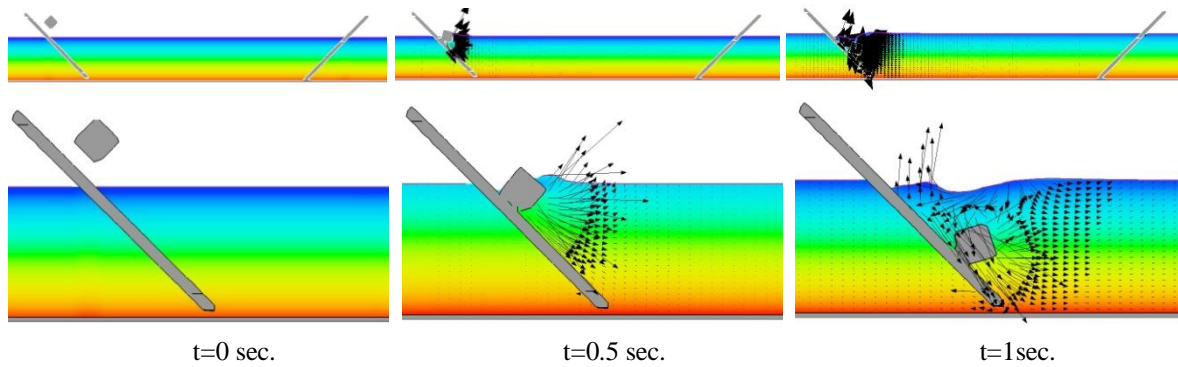


Figure 11. Numerically-derived wave amplitudes for different landslide geometries at  $y=7 m$

If their fitness value is more suitable, then they have more chances to reproduce. This is repeated until some condition (e.g. number of populations or improvement of the best solution) is satisfied. This algorithm can be represented as Figure 1.

Velocity vectors at  $t=0$ ,  $t=0.5$  and  $t=1$  sec. for subaerial deformable rectangular landslide geometry (cross section B-B) is shown in Figure 12.



**Figure 12. Velocity vectors for subaerial deformable rectangular landslide geometry**

Velocity vectors at t=0, t=0.5 and t=1 sec. for submarine Non-deformable rectangular landslide geometry is shown in Figure 13.

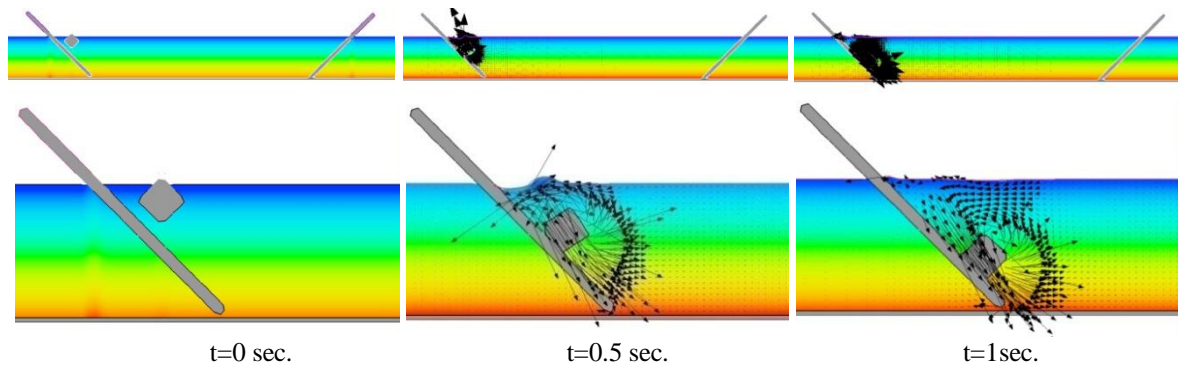


**Figure 13. Velocity vectors for submarine Non-deformable rectangular landslide geometry**

Velocity vectors at t=0, t=0.5 and t=1 sec. for submarine deformable rectangular landslide geometry is shown in Figure 14.

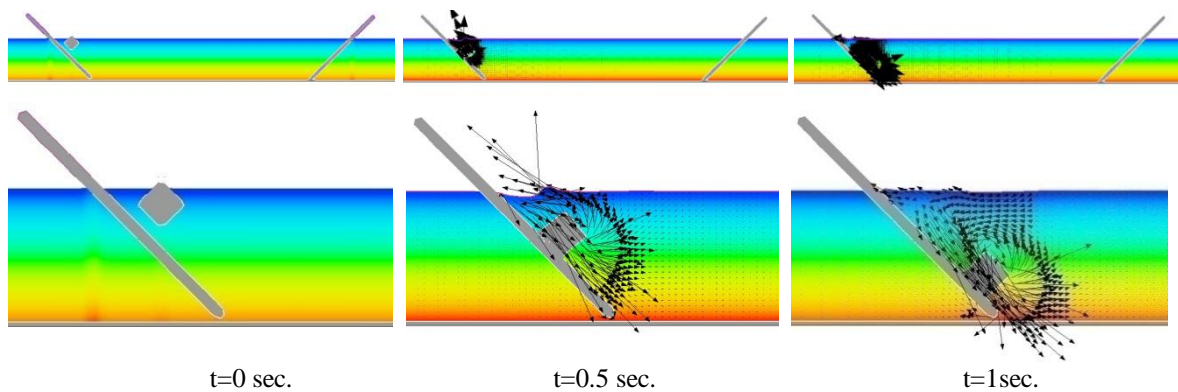


**Figure 14. Velocity vectors for submarine deformable rectangular landslide geometry**

The time series of the free surface elevation at y=8 m for submarine deformable rectangular landslide geometry and submarine non-deformable rectangular landslide geometry are shown in figure 15.

The generated wave is a solitary-like wave with small trailing waves. The calculated maximum and minimum wave heights at both stations show the difference of deformable and non-deformable rectangular geometries. However, figure 15 shows a slight phase difference together. So the deformable and non-deformable are changed less than 9%.

Table 2. shows the variation of water surface elevation (wave) for submarine deformable rectangular landslide geometry and submarine non-deformable rectangular landslide geometry obtained from Flow-3D models for 10 sec.

**Table 2. Variation of water surface elevation (wave) for submarine deformable rectangular landslide geometry and submarine non-deformable rectangular landslide geometry obtained from Flow-3D models for 10 sec.**

Time (sec)	0	1	2	3	4	5	6	7	8	9	10
Surface (m) (non deformable land slide)	120.0	118.5	121.0	119.3	120.3	120.2	119.9	119.7	119.6	120.4	120.0
Surface (m)(deformable land slide)	120.0	119.0	120.4	119.5	120.1	120.3	120.3	119.6	119.5	120.3	119.9

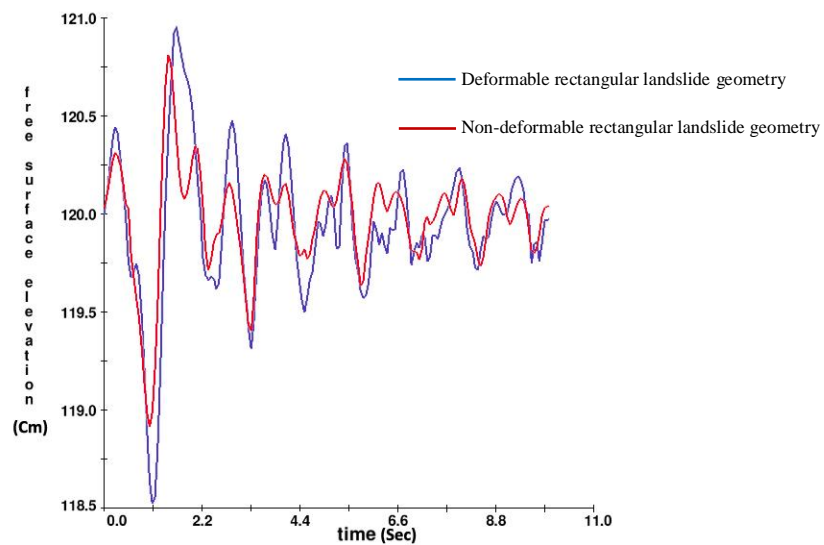


**Figure 15. Time histories of free surface elevation at y=8 m obtained from Flow-3D models.**

The time series of mean kinetic energy for submarine deformable rectangular landslide geometry and subaerial non-deformable rectangular landslide geometry are shown in Figure 16.

Numerical results of mean kinetic energy over time in locations of y=7 m for submarine deformable rectangular landslide geometry and submarine non-deformable rectangular landslide geometry are shown in Figure 16.

It is shown that the maximum mean kinetic energy have the highest and lowest values in non-deformable and deformable rectangular landslide geometry, respectively.

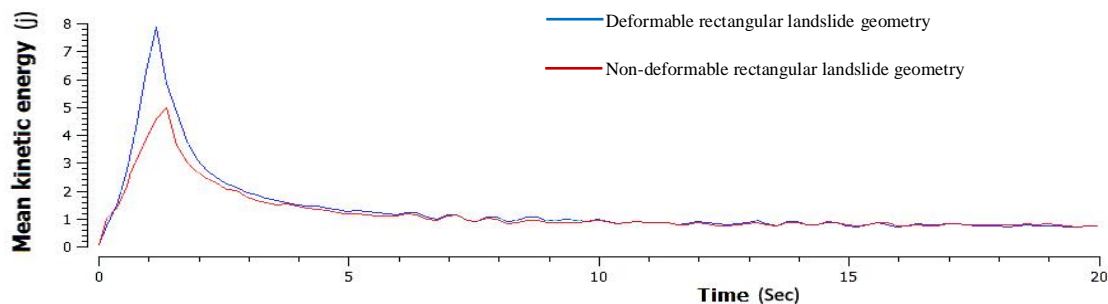


**Figure 16. Time histories of mean kinetic energy obtained from Flow-3D models.**

### 3.3. Case Study

In this work, Subaerial Landslide Generated Waves (SLGW) generation and propagation are studied numerically for a real case. The Dam reservoir, in the north of Iran, is considered as the case study (Figure 17).

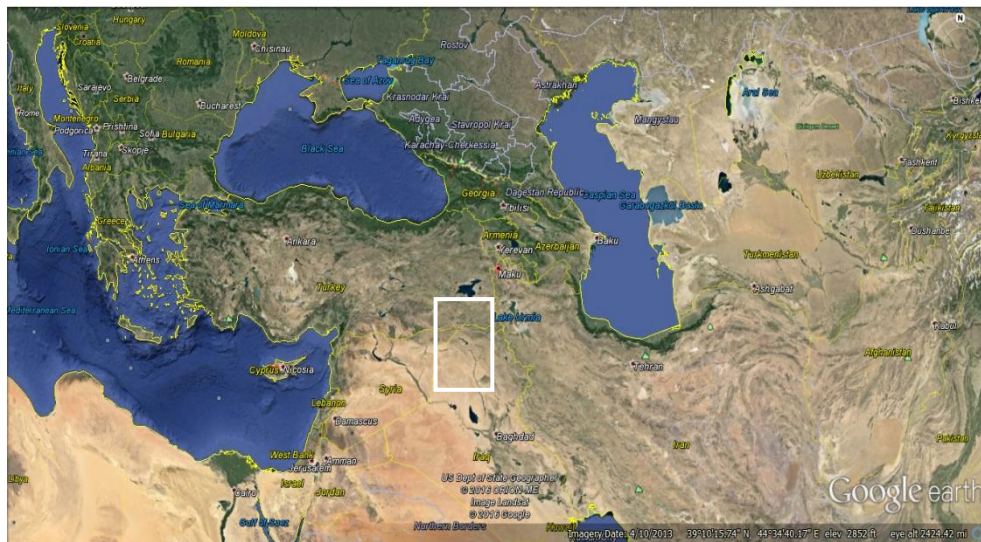


Figure 17. The Google map view of Maku dam

Maku (Barun) dam is located in the north part of Maku town, west Azarbaijan province, Iran, in 11°39'17" north latitude and 44°28'55" east longitude, on the Zangmar River. The Zangmar River originates in the mountains above Maku, along the Turkish-Iranian border, not far from Mount Ararat and flows south and east into the Araxes at the town of Pol Dasht (Figure 18).



Figure 18. Location of the Maku dam, 11°39'17" N and 44°28'55" E. (Google earth map)

Maku dam is 75 m high storage earth dam, with a reservoir capacity of 137 Mm<sup>3</sup> (Figure 19). Length and width of dam are 350 m and 10 m respectively. The dam crest level is 1699 m from sea level (Figure 20b).



Figure 19. Top view of Maku dam reservoir

The dam is located in a seismic region (Figure 20a). The Badavli fault is located near the dam site; thus, seismic conditions intensify its crucial landslide-susceptibility status.

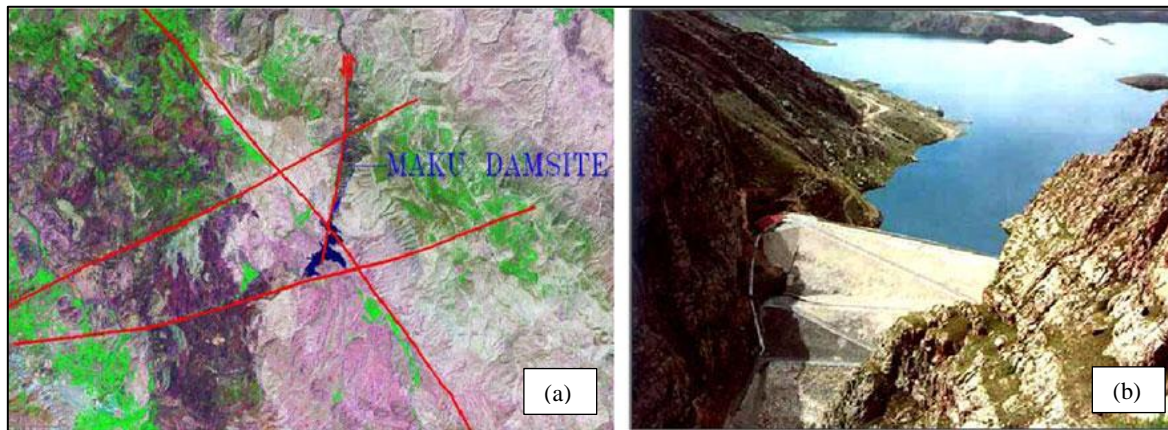


Figure 20. (a) Satellite image of the Maku dam site and the existing faults. (b) An oblique view of the Maku dam

According to geological investigations, multiple factors such as rainfall, successive freezing– melting, pore water pressure changes, sequential changes in underground water level and weathering initiate the formation and extension of large number of tensile cracks along the Maku reservoir beaches (Figure 21.b), which form some areas of instability. One of the most dangerous areas of instability is located on the West beach with the horizontal distance of 235 m from the dam axis (Figure 21.c, d). Another significant area of instability is a circular shape instability located on the Eastern beach with the horizontal distance of 230 m from the dam axis (Figure 21.a).

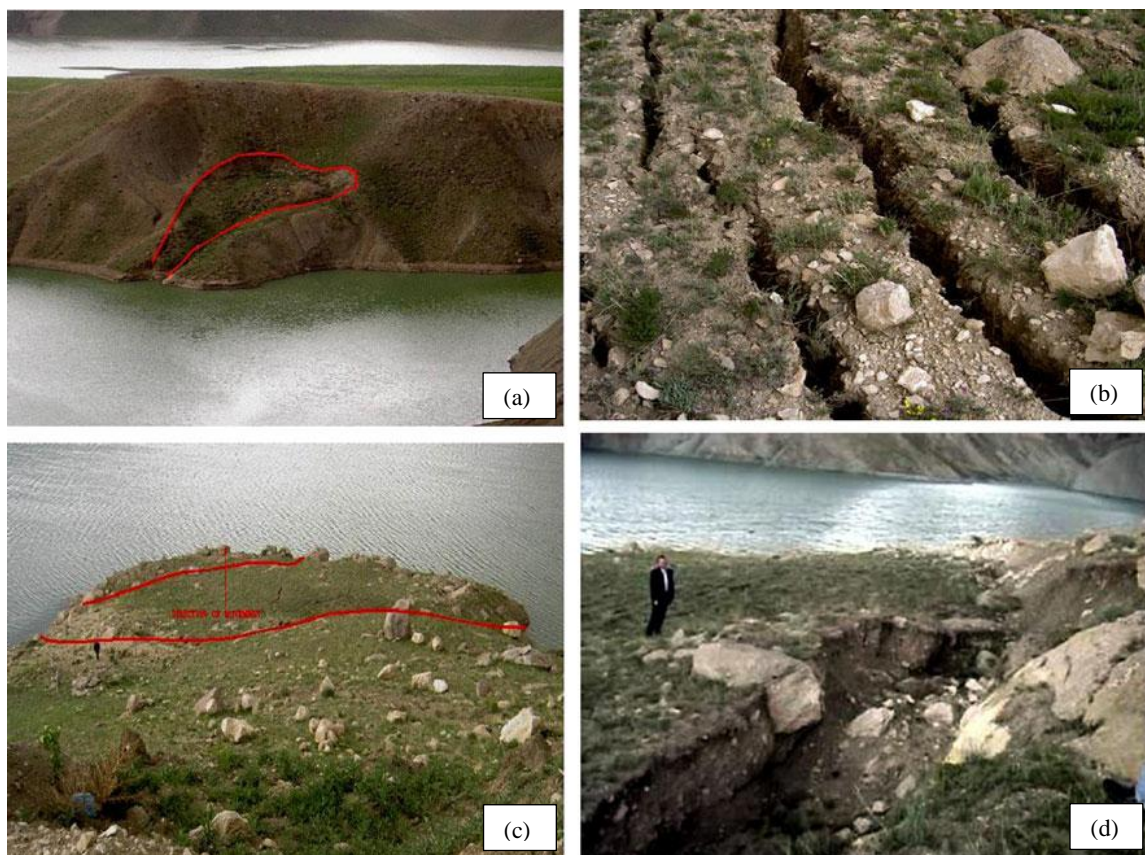


Figure 21. (a) A possible slide on the east bank of the Maku dam reservoir, and (b) its zoom-view. (c) A possible slide on the west bank of the Maku dam reservoir, and (d) its zoom-view

According to the topographic map of the Maku dam site, the landslide on the East beach is subaerial. This means that the center of gravity is above the water surface for the second one. Landslide blocks in both scenarios are partly submerged and proper cases for simulation by the extended numerical model.

The landslide can potentially generate a tsunami. In this paper, we describe the landslide and water wave surface

modeled with flow3D software (Figure 22).

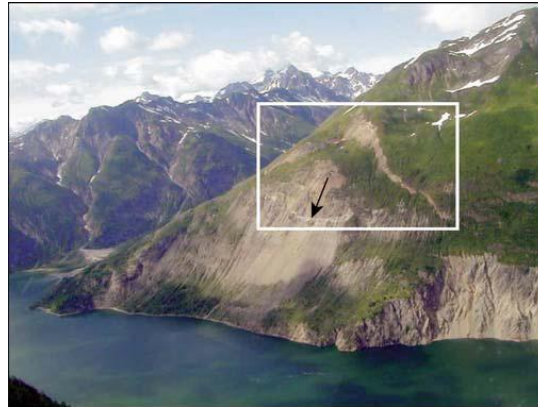


Figure 22. Landslide perched above the shore of Maku dam with white box

### 3.4. Simulation set up

Numerical models were set-up with Flow-3D software. The simulation in this study is performed in rigid subaerial landslide. The volume of rigid slide is  $3.68 \text{ m}^3$ . Mass density of the rigid slide defined  $2 \text{ kg/m}^3$ . Table 3 shows some information about the total mesh size and the typical sizes of the grid elements. Also total number of real cells is 2,400,000. The CPU time used in each simulation is 64 hour. In this study we used viscous flow and laminar model for simulations.

Table 3. Grid information for mesh blocks

Mesh Information	X direction	Y direction	Z direction
Number of real cells	180	140	95
Minimum cell size (m)	1	1	1
Maximum cell size (m)	3	2	2

Figure 23. shows the topographic view of dam reservoir:

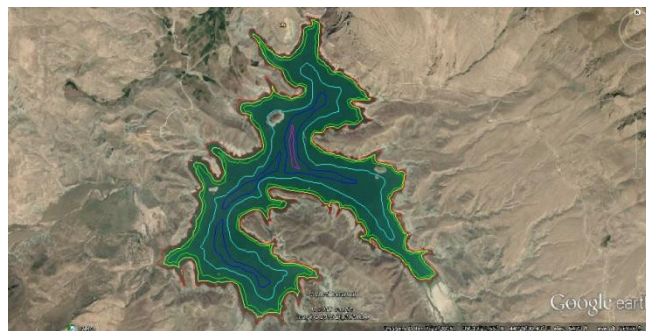


Figure 23. Topographic view of dam reservoir

Figure 24. shows 3D modeling of dam reservoir.

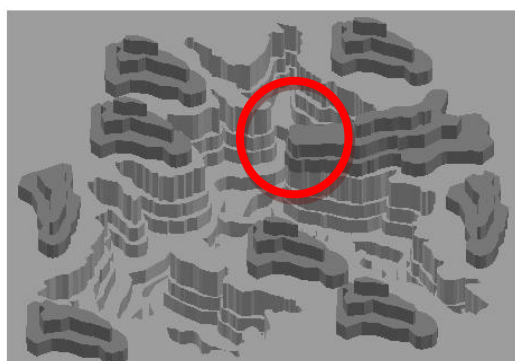


Figure 24. 3D view of dam reservoir

Figure 25. shows 3D modeling of Subaerial slide. This Figure shows subaerial rigid slide by red color and two cross section of A-A and B-B. The height of this right slide is about 2m, 2m width and 1m depth.

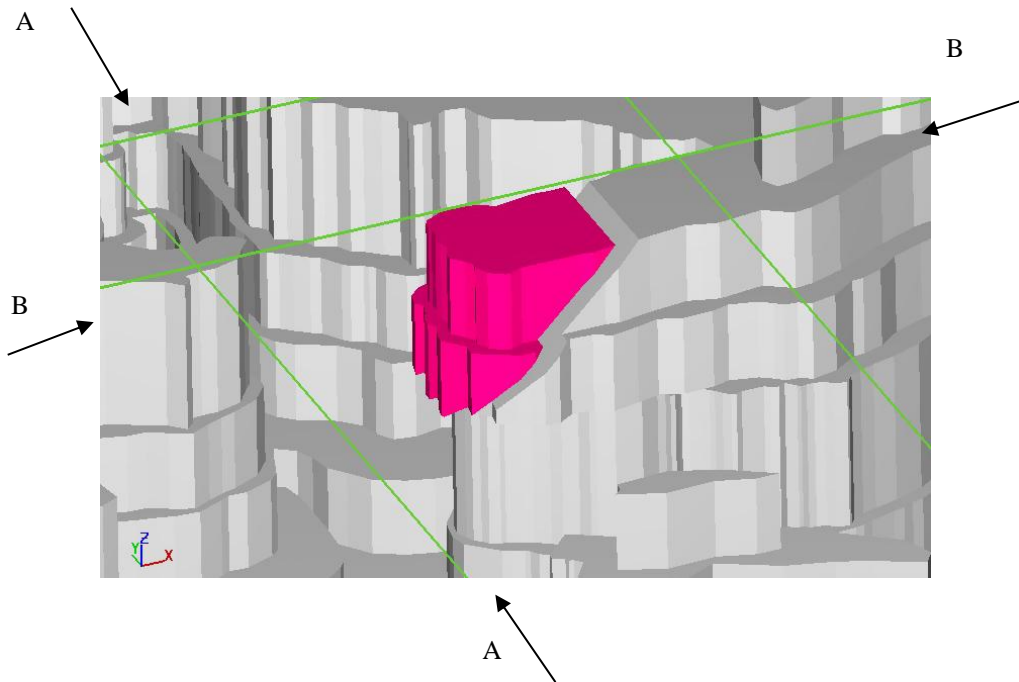


Figure 25. 3D view of dam reservoir and subaerial rigid slide ( $V=3.68 \text{ m}^3$ )

Figure 26. shows 3D modeling of dam reservoir, modeled and analyzed with Flow3D software.

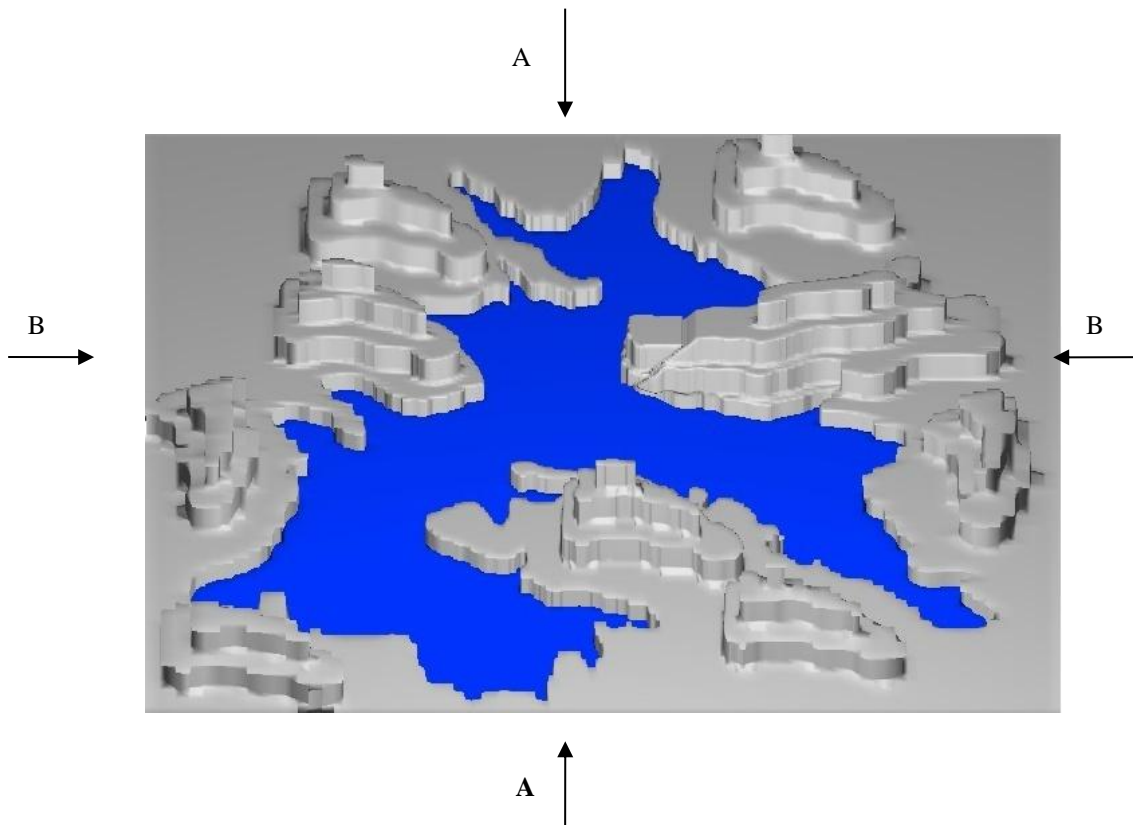
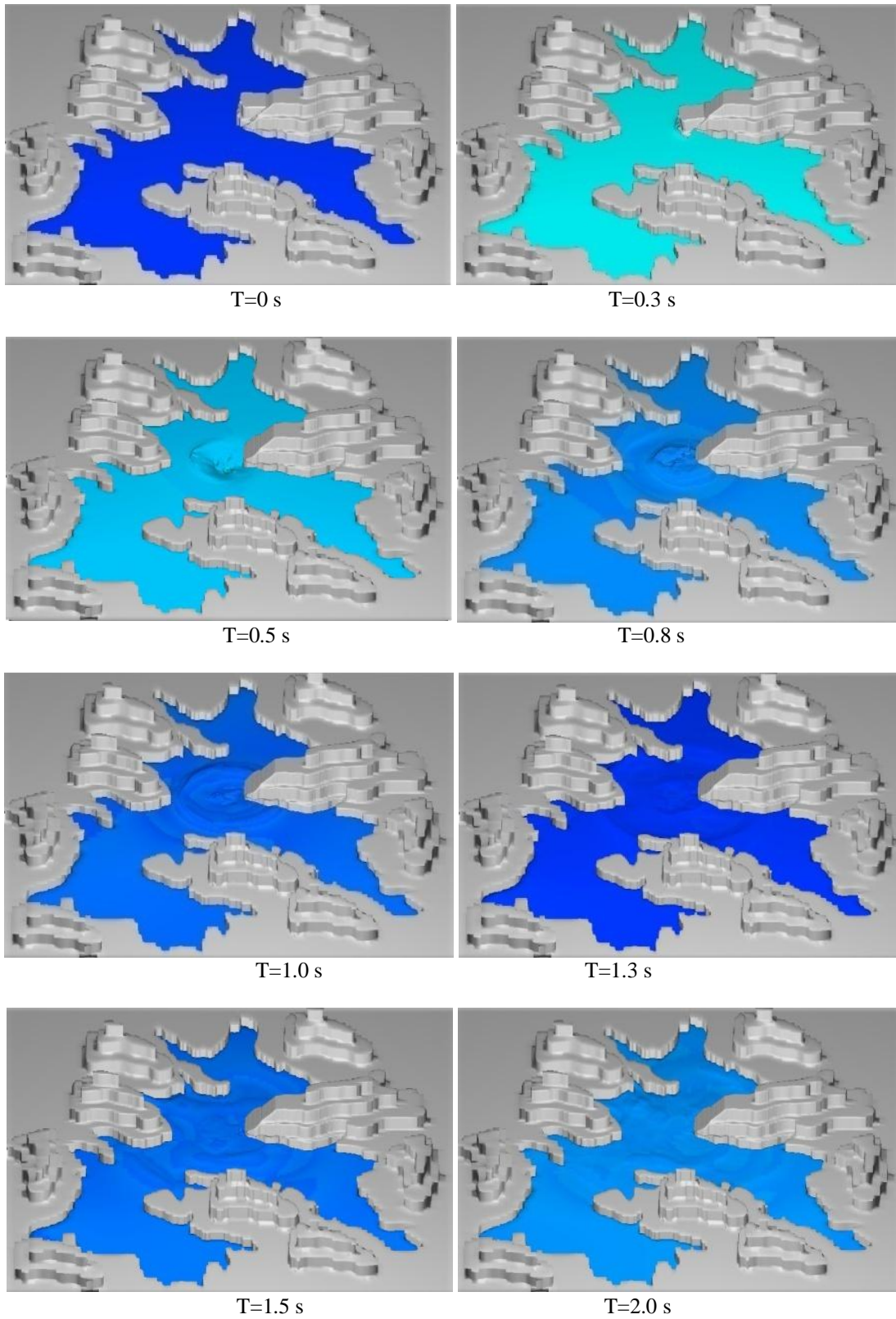
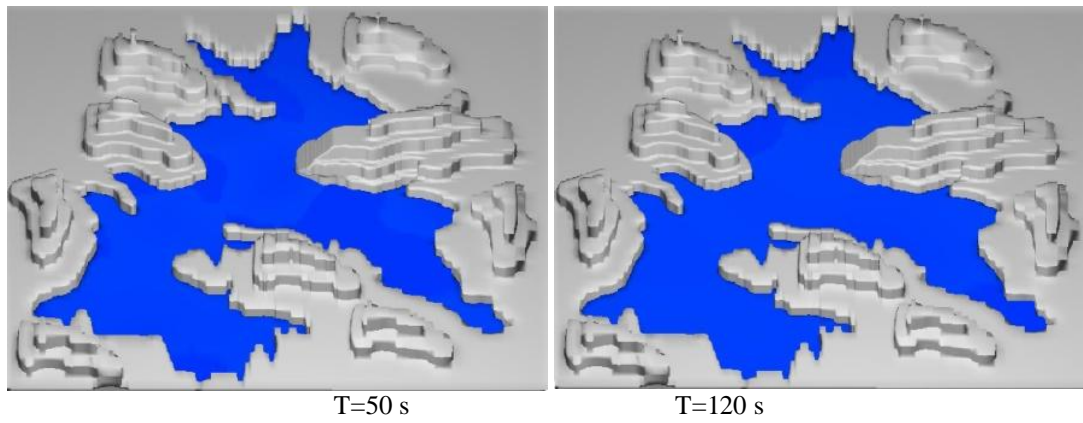


Figure 26. 3D view of dam reservoir modeled with Flow3D software

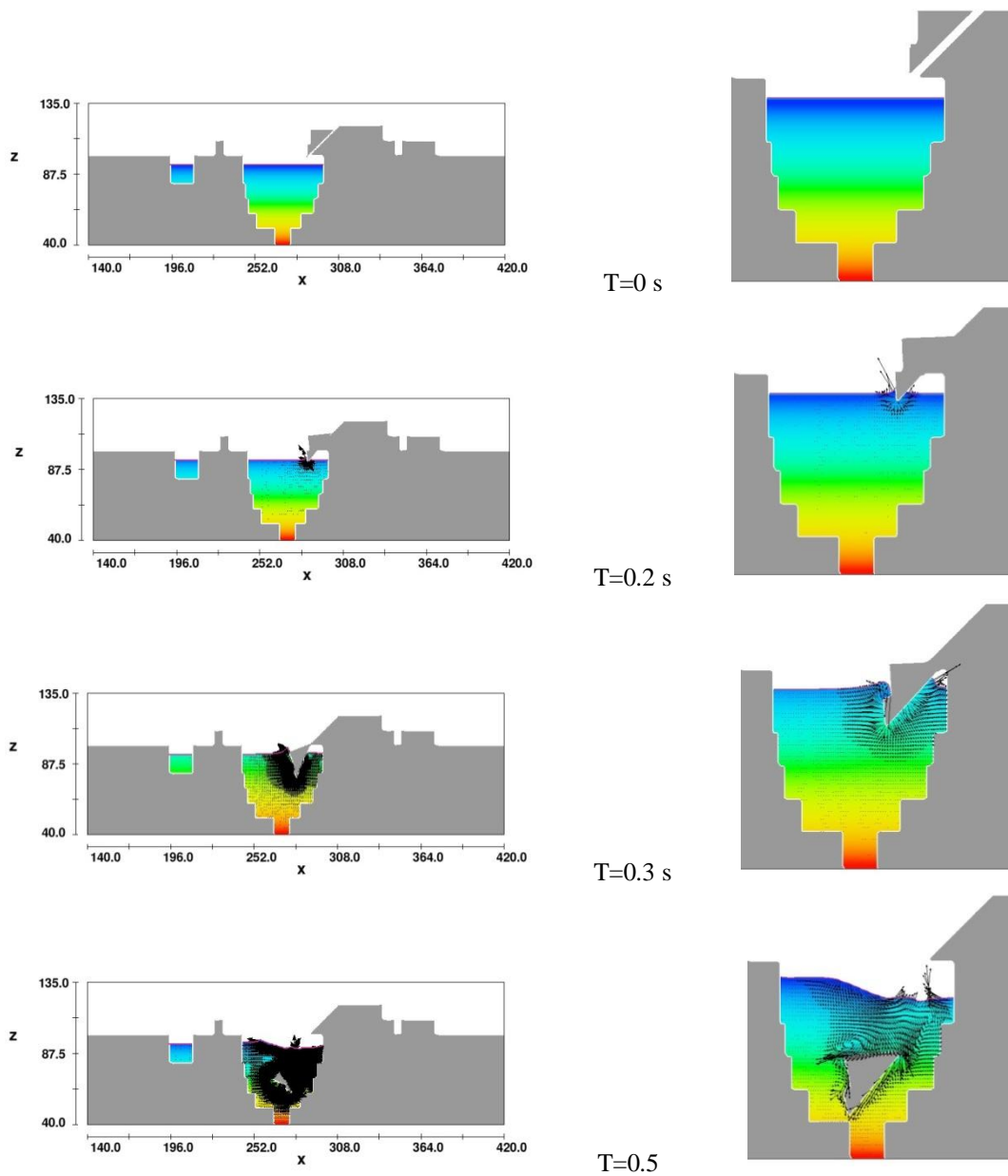
3D views of land sliding at  $t=0$ ,  $t=0.3$ ,  $t=0.5$ ,  $t=0.8$ ,  $t=1$ ,  $t=1.3$ ,  $t=1.5$ ,  $t=2$ ,  $t=50$  and  $t=120$  sec. for subaerial landslide is shown in Figure 27.





**Figure 27. 3D views of land sliding for subaerial landslide at different times**

Figure 28. shows velocity vectors at  $t=0$ ,  $t=0.2$ ,  $t=0.3$ ,  $t=0.5$ ,  $t=0.7$ ,  $t=1.5$ ,  $t=10$ ,  $t=50$ ,  $t=100$  and  $t=120$  sec. for subaerial landslide.



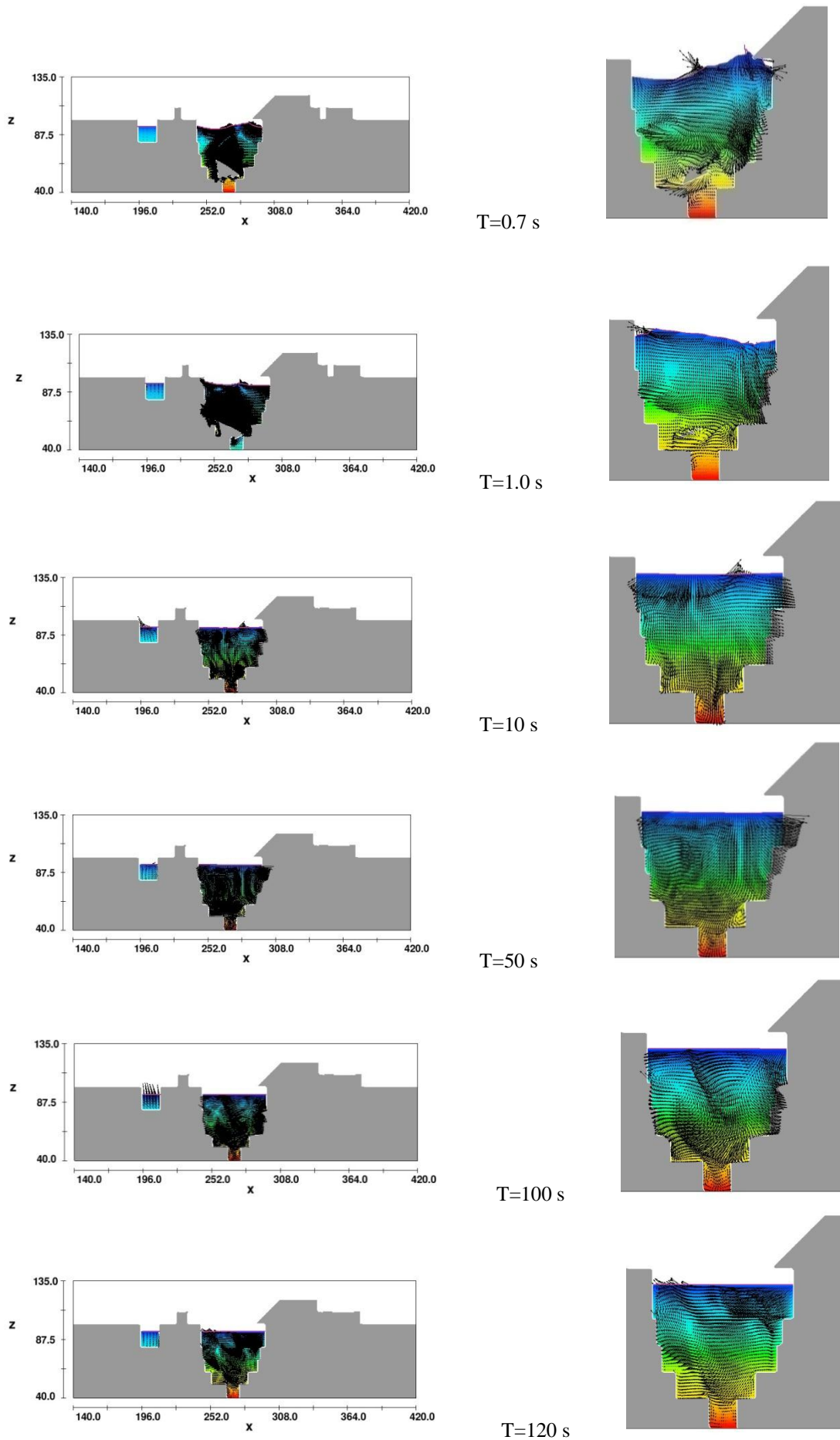
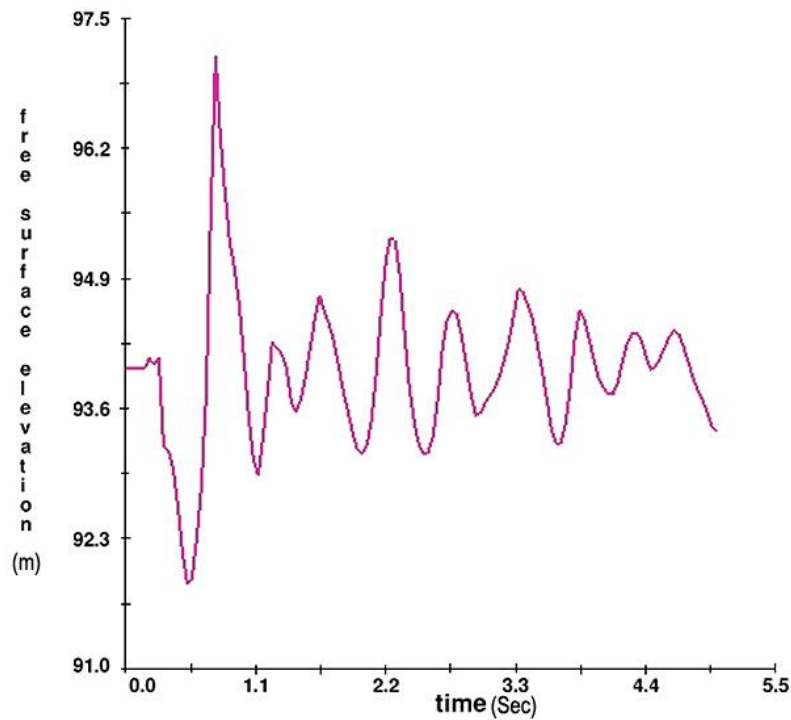


Figure 28. Velocity vectors for subaerial landslide at different times (cross section B-B)

Numerical results of wave amplitudes over time in locations of X=158 m for subaerial landslide is presented in Figure 29. It is shown that the wave amplitude and time histories of free surface elevation.



**Figure 29. Time histories of free surface elevation at X=158 m (cross section A-A) obtained from Flow-3D models**

Numerical results of wave amplitudes over time in locations of X=158 m for subaerial landslide is presented in Figure 30. It is shown that the wave amplitude and time histories of free surface elevation for 50 sec.

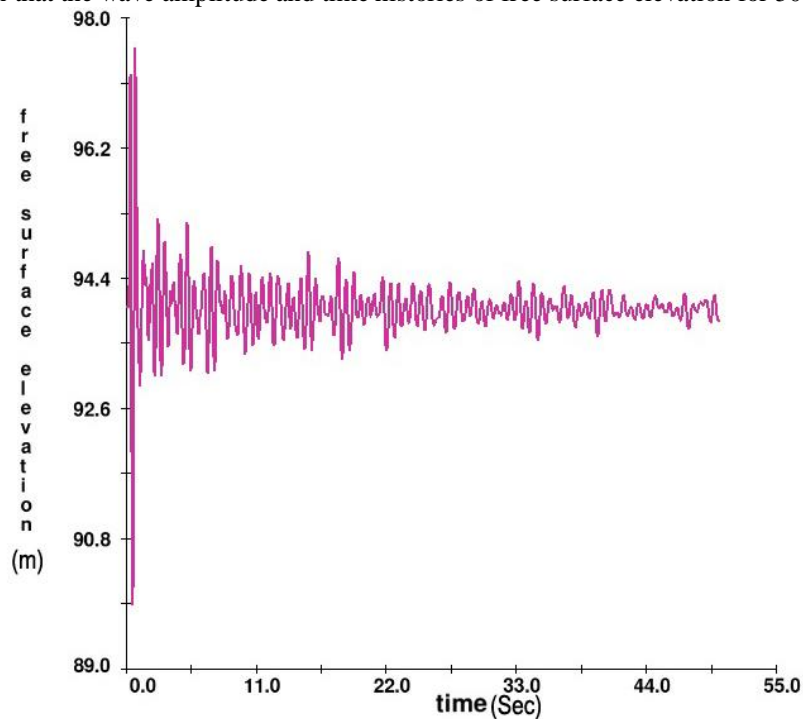


**Figure 30. Time histories of free surface elevation at X=158 m (cross section A-A) obtained from Flow-3D models for 50 sec.**

Numerical results of wave amplitudes over time in locations of X=158 m for subaerial landslide is presented in Figure 31. It is shown that the wave amplitude and time histories of free surface elevation for 120 sec.

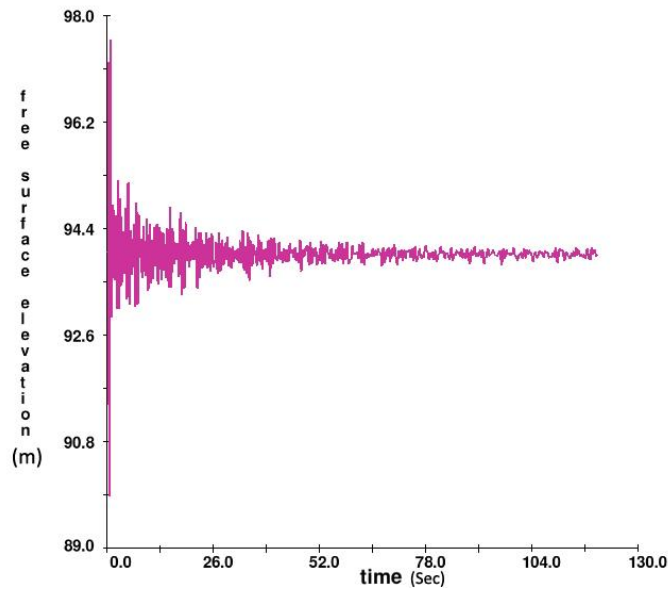


Figure 31. Time histories of free surface elevation at X=158 m (cross section A-A) obtained from Flow-3D models for 120 sec.

In the literature of landslide generated impulse waves two different slide energies were introduced in comparisons with the generated wave energy: the potential slide energy before slide release and the kinetic slide energy upon impact. A simple estimate is the potential energy of a slide, which has been used by Miller analyzing slides in the field. The potential slide energy was applied to laboratory generated impulse waves by Johnson and Bermel and Wiegel. The conversion from potential to kinetic energy upon impact may vary significantly among both laboratory studies and observed events due to different friction losses. The potential slide energy before release does not determine the kinetic slide impact energy. Therefore the kinetic slide impact energy was used in the following analysis of the slide to wave energy conversion.

Numerical results of wave energy over time for subaerial landslide are presented in Figure 32. It is shown that the wave energy and time histories for 120 sec.

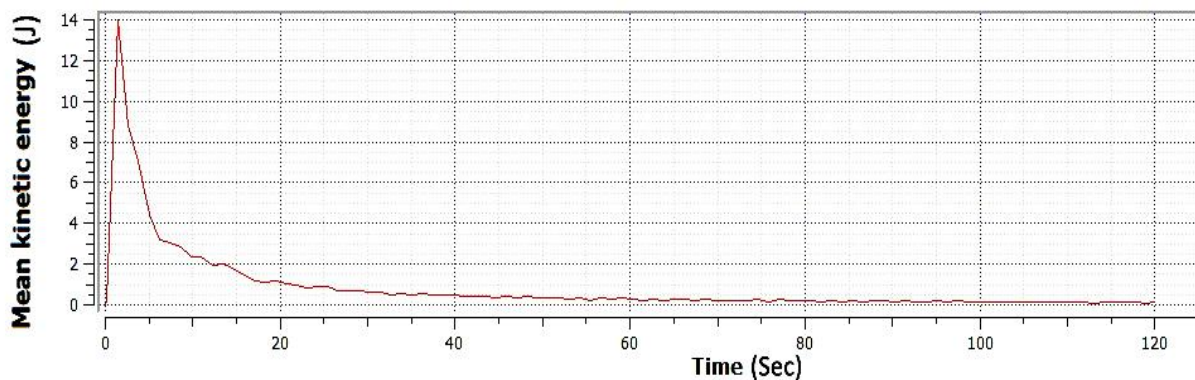


Figure 32. Time histories of wave energy obtained from Flow-3D models for 120 sec.

### 3.5. Velocity vectors

Table 4. shows variation of velocity vectors and water surface elevation (wave) obtained from Flow-3D models for 100 seconds.

Table 4. Variation of velocity vectors and water surface elevation (wave) obtained from Flow-3D models for 100 sec.

Time (sec)	0	10	20	30	40	50	60	70	80	90	100
U (m/s)	0	-2.3	3.2	0.5	0.3	1.1	-4.2	3	0	-0.6	0.7
V (m/s)	0	-1.8	-2	1.6	1.4	0	0.5	2	1.8	0	-0.4
W (m/s)	0	-8	1.5	1.1	-0.2	4.3	-0.9	3.7	-0.7	-0.6	-1.6
Water Surface (m)	94	93.7	94.1	93	94.4	93.8	93.9	93.6	94.1	94.4	93.5

Figure 33. shows Variation of velocity vectors (u, v, w) obtained from Flow-3D models for 120 seconds.

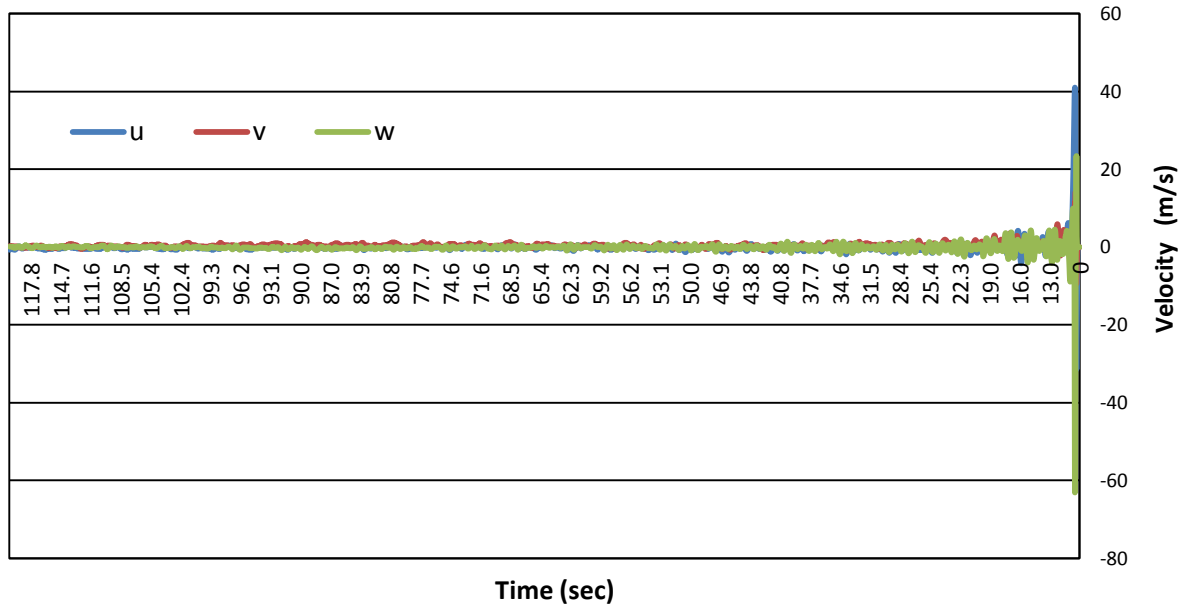


Figure 33. Variation of velocity vectors (u, v, w) obtained from Flow-3D models for 120 seconds.

Table 5. shows variation of velocity vectors and water surface elevation (wave) obtained from Flow-3D models for 1.0 second. This table shows that the maximum level of water surface occurred at t=0.8 second and the minimum level of water surface occurred at t=0.5 second.

Table 5. Variation of velocity vectors and water surface elevation (wave) obtained from Flow-3D models for 1.0 sec.

Time (sec)	0	0.1	0.2	0.3	0.4	0.5	0.6	0.7	0.8	0.9	1.0
U (m/s)	0	0	-0.5	-21	38.1	38.0	19.6	10.5	6.7	-2.9	-2.3
V (m/s)	0	0	-0.1	-5.0	6.6	9.0	5.8	3.6	2.5	-0.2	-1.8
W (m/s)	0	0	0	2.7	-52	-11	9.8	8.6	5.8	-5.9	-8
Water Surface (m)	94	94	94	94.9	93.4	89.8	92.1	95.3	97.6	95.6	93.7

Figure 34. shows Variation of velocity vectors (u, v, w) obtained from Flow-3D models for 1.0 second.

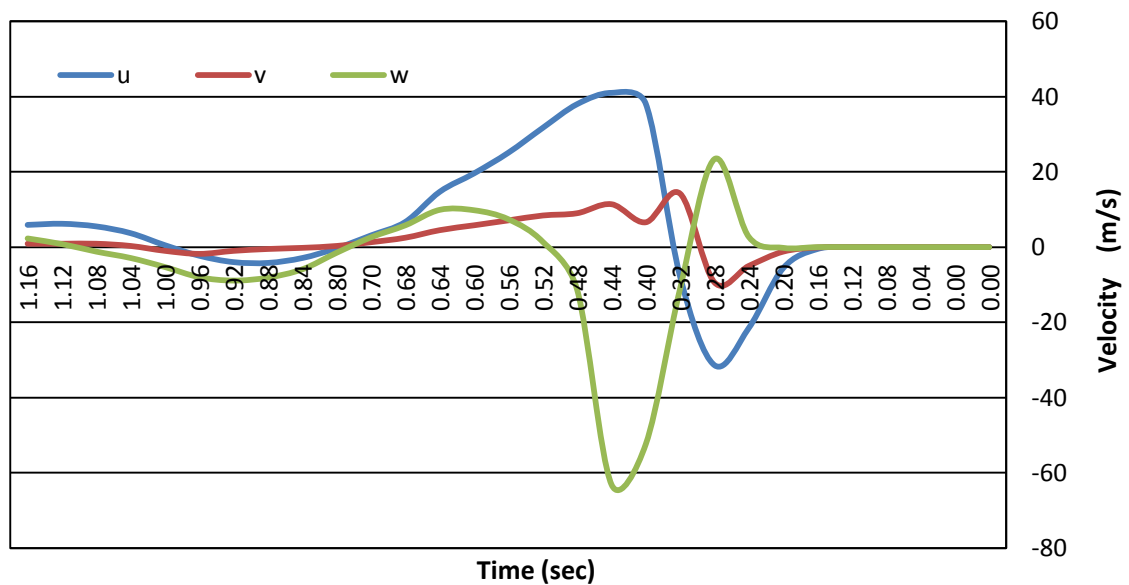


Figure 34. Variation of velocity vectors (u, v, w) obtained from Flow-3D models for 1.0 second

### 3.6. Dam overtopping

The levels of the Maku dam crest and the normal water are 1,690 and 1,680 m, respectively. A height of 1 m is estimated for the wind- and earthquake-generated waves. Thus, the dam freeboard is 9 m. In rainy seasons, the water level can rise close to the spillway level. The spillway of the Maku dam is a tunnel spillway in the left sidewall with a diagonal shaft, located at a level of 1,685 m. As it is more probable that landslides may initiate in rainy seasons, we consider the best (water level of 1,680 m) and the worst (water level of 1,685 m) conditions for estimating dam overtopping. The volume of overtopping water is calculated with the Equation 13. (Fritz et al. 2004):

$$V = b \int \eta dx = b C_c \int \eta dt \quad (13)$$

where  $V$  is the dam overtopping volume,  $b$  the dam crest length,  $\eta$  the positive wave amplitude over the dam crest level,  $c_c$  the wave crest propagation velocity and  $x$  and  $t$  the distance and the time interval during which the wave height close to the dam is higher than the dam crest level, respectively. The time series of water surface fluctuations is shown in Figure 31.

The maximum wave heights close to the dam body is 3.6 m. Thus, in the best condition, no overtopping happens. And also in the worst condition (the rainy seasons), no overtopping happens. Therefore, it seems that the 9 m freeboard of the Maku dam is enough to prevent overtopping a huge volume of water due to the considered landslide.

## 4. Conclusion

The effects of the main parameters such as, impact velocity, slide geometry, shape and deformation on the impulse wave characteristics have been inspected. And Laboratory investigations have been performed on the impulsive waves caused by subaerial and submarine landslide. Numerical analyses were performed to simulate the wave generation due to subaerial and submarine landslide. Different types of landslide geometries were used to analyze the flow field. Simulated results show complex flow patterns in the lake in terms of velocity field, and free surface profiles. Numerical results of wave amplitudes and velocity magnitudes for circular, rectangular and triangular landslide geometries are applied to the sliding materials are computed, which are used by geotechnical engineers to study the stabilization of the slope. On the basis of the obtained results, the following conclusions can be drawn:

- Circular landslide behavior compared with rectangular and triangular shapes during wave propagation, hence it is expected that the wave amplitude have the highest and lowest values in triangular, rectangular and circular shapes, respectively.
- Also we obtain the circular shape has lowest value of wave amplitude, and triangular shape has highest wave amplitude during in this modeling and triangular landslide has the most absolute values of horizontal and vertical forces during and after the initial wave generation.

The extended model is applied for simulating real case, the Maku dam reservoirs located in the northwestern of Iran. The generated wave heights, wave run-up, maximum wave height above the dam crest, and the dam overtopping volume have been evaluated for each case.

The maximum wave heights close to the dam body is 3.6 m. Thus, in the best condition, no overtopping happens. And also in the worst condition (the rainy seasons), no overtopping happens. Therefore, it seems that the 9 m freeboard of the Maku dam is enough to prevent overtopping a huge volume of water due to the considered landslide.

## 5. References

- [1] Wiegel RL, Laboratory studies of gravity waves generated by the movement of a submarine body. *Trans Am Geophys Union* 1955;36(5):759–74.
- [2] Heinrich P, Nonlinear water waves generated by submarine and aerial landslides. *J Waterways, Port, Coast, Ocean Engng* 1992; 118(3):249–66.
- [3] Watts P, Water waves generated by underwater landslides. PhD thesis, California Institute of Technology, Pasadena, CA, 1997.
- [4] Iwasaki S, The wave forms and directivity of a tsunami generated by an earthquake and a landslide. *Sci Tsunami Hazards* 1997; 15:23–40.
- [5] Jiang L, Leblond PH. The coupling of a submarine slide and the surface waves which it generates. *J Geophys Res* 1992; 97(8):12 731–44.
- [6] Verriere M, Lenoir M. Computation of waves generated by submarine landslides. *Intl J Num Methods Fluids* 1992; 14:403–21.
- [7] Harbitz CB, Model simulations of tsunamis generated by the Storegga slides. *Marine Geol* 1992;105:1–21.
- [8] Heller V, Landslide generated impulse waves, Prediction of near field characteristics, Zürich, 2008.
- [9] Moalemi M, the effects of geometry on landslide generated tsunamis, June 2010, University of Southampton

- [10] Heller V, Willi H. Hager, F.ASCE2, Impulse Product Parameter in Landslide Generated Impulse Waves, journal of waterway, coastal, and ocean engineering , May/June 2010
- [11] Ataie-Ashtiani B, Najafi-Jilani A. Laboratory investigations on impulsive waves caused by underwater landslide, Department of Civil Engineering, Sharif University of Technology, April 2008
- [12] Mohammed F, Physical modeling of tsunamis generated by three-dimensional deformable granular landslides, Georgia Institute of Technology October 2009
- [13] Ataie-Ashtiani B, and Malek-Mohammadi S, Mapping impulsive waves due to subaerial landslides into a dam reservoir, Department of Civil Engineering, Sharif University of Technology, 2008
- [14] Ataie-Ashtiani B, and Shobeyri G, Numerical simulation of landslide impulsive waves by incompressible smoothed particle hydrodynamics, Department of Civil Engineering, Sharif University of Technology, Tehran, Iran, May 2007
- [15] Grilli S, and Watts P, Modeling of waves generated by a moving submerged body. Applications to underwater landslides, Ocean Engineering Department, University of Rhode Island, Narragansett, RI 02882, USA, 19 July 1999
- [16] FLOW 3D software ver.10, Flow Science, Inc., FLOW-3D and VOF are registered in the US Patent and Trademark Office, flow 3d User Manual ver.9.3 Copyright 2008, Web site: www.flow3d.com
- [17] Jiang, Lin, and Paul H. LeBlond. "Three-dimensional modelling of tsunami generation due to a submarine mudslide." Journal of physical oceanography 24, no. 3 (1994): 559-572.
- [18] Imamura, Fumihiko, and Edison C. Gica. "Numerical model for tsunami generation due to subaqueous landslide along a coast." Sci. Tsunami Hazards 14, no. 1 (1996): 13-28.
- [19] Tappin, D. et al., Sediment slump likely caused 1998 Papua New Guinea tsunami, EOS 80, 329, 334, 340. 1999.
- [20] Heinrich, P., Piatensi, A., Okal, E., and Hébert, H.: 2000, Near-field modeling of the July 17, 1998 tsunami in Papua New Guinea, Geophys. Res. Let. 27, 3037-3040.
- [21] Altinok, Y., Alpar, B., Ersoy, S. and Yalciner, A.C., Tsunami generation of the Kocaeli Earthquake (August 17th, 1999) in the Izmit Bay: Coastal observations, bathymetry and seismic data, Turkish J. Marine Sciences 5 (3), 131-148, 1999.
- [22] Kulikov, E.A., Rabinovich, A.B., Thomson, R.E., and Bornhold, B.D.: 1996, The landslide tsunami of November 3, 1994, Skagway Harbor, Alaska, J. Geophys. Res. 101 (C3), 6609-6615.
- [23] Kowalik, Z., Landslide-generated tsunami in Skagway, Alaska, Science of Tsunami Hazards 15 (2), 89-106, 1997.
- [24] Rabinovich, A.B., Thomson, R.E., Kulikov, E.A., Bornhold, B.D., and Fine, I.V.: 1999, The landslide-generated tsunami of November 3, 1994 in Skagway Harbor, Alaska: A case study, Geophys. Res. Let. 26, (19), 3009-3012.
- [25] LeBlond, P.H. and Jones, A.T., Underwater landslides ineffective at tsunami generation, Science of Tsunami Hazards 13 (1), 25-26, 1995.
- [26] Miller, D.J.: 1960, The Alaska Earthquake on July 10, 1958: Giant wave in Lituya Bay, Bull. Seism. Soc. America 50 (2), 253-266.
- [27] Lander, J.F.: 1996, Tsunamis Affecting Alaska, 1737-1996. Boulder, US Dep. Comm., 195 p.
- [28] Raichlen, F., J.J. Lee, C. Petroff, and P. Watts, 1996: The generation of waves by a landslide: Skagway, Alaska: A case study, Proc. 25th Coastal Eng. Conf., ASCE, Orlando, Florida, 1478-1490.
- [29] Jiang, L. and LeBlond, P.H., the coupling of a submarine slide and the surface waves which it generates, J. Geophys. Res. 97 (C8), 12,731-12,744, 1992.
- [30] Fine, I.V., Rabinovich, A.B., Kulikov, E.A., Thomson, R.E., and Bornhold, B.D.: 1998, Numerical modelling of landslide-generated tsunamis with application to the Skagway Harbor tsunami of November 3, 1994, Proc. Int. Conf. on Tsunamis, Paris, 211-223.
- [31] Thomson, R.E., Rabinovich, A.B., Kulikov, E.A., Fine, I.V., and Bornhold, B.D., On numerical simulation of the landslide-generated tsunami of November 3, 1994 in Skagway Harbor, Alaska, in Tsunami Research at the End of a Critical Decade, edited by G. Hebenstreit, Kluwer, Dordrecht, 243-282, 2001.
- [32] Titov, V.V., and González, F., Numerical study of the source of the July 1998 PNG tsunami, in Tsunami Research at the End of a Critical Decade, edited by G. Hebenstreit, Kluwer, Dordrecht, 197-207, 2001.
- [33] Imamura, F., Hashi, K., and Imteaz, Md.M.A., Modeling for tsunamis generated by landsliding and debris flow, in Tsunami Research at the End of a Critical Decade, edited by G. Hebenstreit, Kluwer, Dordrecht, 209-228, 2001.
- [34] Assier-Rzadkiewicz, S., Heinrich, P., Sabatier, P.C., Savoye, B., and Bourillet, J.F., Numerical modelling of landslide-

generated tsunami: The 1979 Nice event, *Pure Appl. Geophys.* 157, 1707-1727, 2000.

[35] Heinrich, P., Nonlinear water waves generated by submarine and aerial landslides, *J. Waterways, Port, Coastal and Ocean Eng.*, ASCE, 118 (3), 249-266, 1992.

[36] Heinrich, P., Mangeney, A., Guibourg, S., Roche, R., Boudon, G., and Vheminée, J.-L., Simulation of water waves generated by a potential debris avalanche in Montserrat, Lesser Antilles, *Geophys. Res. Let.* 25 (19), 3697-3700, 1998.

[37] Norem, H., Locat, J., and Schieldrop B., an approach to the physics and modeling of submarine flowslides, *Mar. Geotechnol.* 9, 93-111, 1991.

[38] Khoolosi, V., Kabdaşlı, S., and Farrokhpour, S., Modeling and Comparison of Water Waves Caused by Landslides into Reservoirs. *Watershed Management 2015*: pp. 72-78. doi: 10.1061/9780784479322.007.

[39] Yavari-Ramshe S, Ataie-Ashtiani B., A rigorous finite volume model to simulate subaerial and submarine landslide-generated waves. *Landslides*. 2015. doi:10.1007/s10346-015-0662-6.